JOURNAL OF APPLIED ELECTROCHEMISTRY 26 (1996)

Electrolytic generation of hydrogen on Pt-loaded porous graphite electrodes from flowing alkaline solutions

M. S. EL-DEAB, M. E. EL-SHAKRE, B. E. EL-ANADOULI, B. G. ATEYA

Chemistry Department, Faculty of Science, Cairo University, Cairo, Egypt

Received 6 July 1995; revised 15 December 1995

The aim of this work was to test the feasibility of using porous graphite electrodes as cathodes for the electrolytic production of hydrogen from flowing alkaline solutions. The platinum loading on the graphite substrate was found to decrease the potential required to sustain a certain rate of hydrogen production, and hence the energy consumed during electrolysis. The experimental i/E relations agreed with those theoretically predicted on the basis of a mathematical model up to a current density of about 200 mA cm^{-2}. The excessive polarization at higher current is attributed to trapping of hydrogen gas bubbles within the porous electrode.

1. Introduction

The electrolysis of water has long been a proven technology for the production of high purity hydrogen [1–4]. Other methods for hydrogen gas production, such as magnetohydrolysis or photohydrolysis are in the early stages of development [5]. The main running cost of the process is the price of the electrical energy used to overcome the various types of polarization which accompany the electrolytic process.

The various components of the cell voltage are given by

$$V_{cell} = \Delta E + \Sigma\eta + iR \quad (1)$$

where ΔE is the thermodynamic cell voltage, $\Sigma\eta$ is the sum of activation and concentration polarizations which accompany the process, and the iR is the ohmic potential drop within the interelectrode gap, the electrode matrix and the outer circuit.

Although the activation polarization, η_{act}, drives the electron transfer process across the electrode/electrolyte interface, the ohmic (iR) polarization sustains the flow of ionic current through the electrolyte, which is often heavily dispersed with gas [1]. The minimization of the cell voltage and, consequently, the energy loss is a prime objective in designing electrodes and cell configurations [1]. This objective may be achieved by operating at high temperature, pressure and electrolyte conductivity [6, 7], and by using highly active electrocatalytic electrode materials [8–10]. In this regard various materials have been suggested for use as cathodes for the electrolytic process, for example, transition metal alloys [9, 11–13], semiconductors and metal oxides [5, 14, 15]. These materials decrease the energy losses, but their prices are prohibitively high.

There are much cheaper fibrous materials, possessing high specific surface areas such as reticulated vitreous carbon (r.v.c.) and graphite felt. Some of these have been used as electrodes in many electrochemical processes, for example, in the removal of heavy metal ions from waste water [16, 17] and in water electrolysis [18].

The purpose of this work is to study the feasibility of using graphite felt as cathode for the hydrogen evolution reaction (h.e.r.) from flowing alkaline solutions and to evaluate the effects of Pt-loading on both the polarization behaviour and the energy consumption during electrolysis. The results are analysed within the framework of a recently developed mathematical model which takes into account the effects of both activation and ohmic polarizations [19].

2. Experimental details

The electrolysis cell was designed to allow flow of the electrolyte through the porous graphite electrode. Figure 1 is a schematic of the electrode chamber in the electrolysis cell. It is similar to the cell used earlier [20] except that the present cell can accommodate fairly thin porous electrodes. The graphite electrode had a diameter of 1.2 cm. It was held down tightly with a rubber cylinder onto the fritted glass disc to prevent it from floating under the hydrostatic pressure of the electrolyte and to ensure good electrical contact to the current collector. An upper part of the cell pressed onto the rubber cylinder. The electrolyte was forced from the bottom (entry face) of the cell using a flow system driven by a constant pressure head. The reacted electrolyte, along with the resulting gas bubbles emerged from the top side (exit face) of the electrode.

The working electrode was polarized using a platinum coil as a counter electrode: this was positioned down-stream with respect to the electrolyte flow. This arrangement facilitated the removal of the gas bubbles which were generated within the working electrode under the combined effects of gas lift and electrolyte flow. Further justifications for this experimental setup and directions of current and electrolyte

0021-891X/93 1996 Chapman & Hall

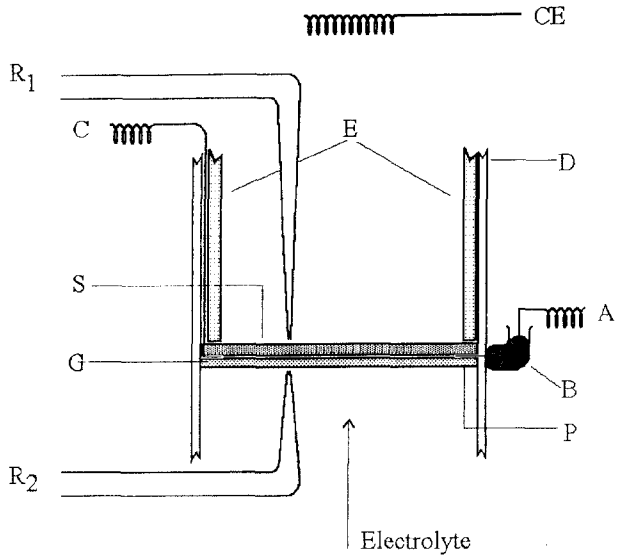

Fig. 1. Diagrammatic representation of the electrode chamber. (A) connection to the current collector, (B) mercury connection, (C) connection to the electrode to test its resistance, (D) cell wall, (E) rubber cylinder, (P) plantinum current collector, (S) working electrode, (G) fritted glass disc, (R_1, R_2) reference electrodes and (CE) counter electrode.

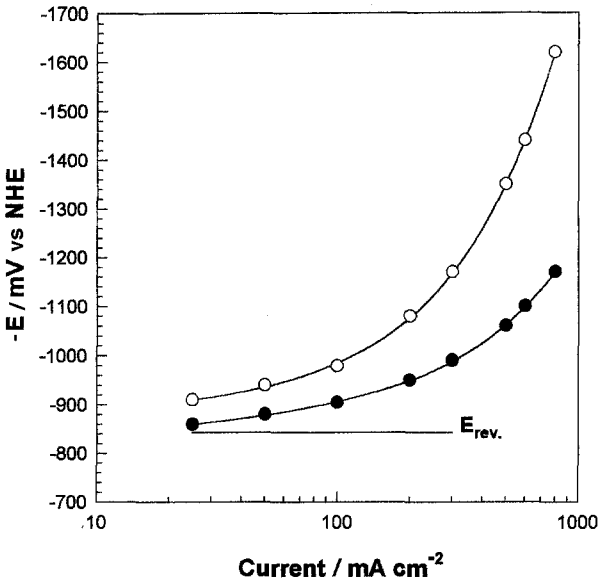

Fig. 2. Current–potential relations for the h.e.r. on Pt-loaded graphite electrode in 5 M KOH at 30 °C flowing at 0.88 cm s^{-1}. Key: (○) E_L and (●) E_o of Pt-loaded graphite.

flow are reported elsewhere [21]. The potentials at both the entry (E_o) and exit faces (E_L) of the electrode were measured using two Hg/HgO/3M KOH reference electrodes (standard potential of 98 mV vs NHE [22]). The Luggin capillaries of the two reference electrodes were positioned close to the electrode surface to minimize the *iR* drop.

The current–potential relations were measured using a simple galvanostatic technique. Current densities were calculated on the basis of the geometrical cross-sectional area of the electrode. Measurements were taken in both ascending and descending directions. No significant hysteresis was observed. The temperature of the electrolyte was adjusted to 30 ± 2 °C. The electrodes were in the form of a Pt-loaded porous graphite felt, of 2 mm thickness. This graphite felt was supplied by the Energy Research Corporation, Danburg, Connecticut, and had the following specifications: the Pt-loading was at 9.73×10^{-3} g Pt cm^{-2} of the geometrical cross-sectional area on only one surface. The SEM revealed that the Pt-loading was uniformly distributed on the electrode surface (see Fig. 4). The graphite substrate had a BET area of about 10 $m^2 g^{-1}$, while the BET area of the Pt-loading was about 50 $m^2 g^{-1}$ of Pt-loading. The resistance of each Pt-loaded graphite electrode was approximately 0.2 Ω in the direction of electrolyte flow per layer of graphite (2 mm thickness).

3. Results and discussion

3.1. *Current–potential relations*

Figure 2 shows the current-potential (i/E) relations for the h.e.r. at an electrode made of Pt-loaded graphite felt. The figure shows the potentials at both the entry (E_o) and exit faces (E_L) of the electrode and the value of the reversible potential ($E_{rev.}$).Increase in current leads to an increase in both E_o and E_L and to an increase in $\Delta E = E_L - E_o$, which is the ohmic drop within the pore electrolyte.

It was found that the flow rate does not affect the current–potential relations for the h.e.r. from flowing alkaline solutions [23]. This indicates that the h.e.r. is not mass transfer controlled. The h.e.r. is represented by the following equation in alkaline medium:

$$2H_2O + 2e^- \longrightarrow 2OH^- + H_2(g) \qquad (2)$$

Since water is always present in large excess, it follows that its concentration does not change significantly within the pores of the electrode. Consequently, the flow of the electrolyte has no effect on the potential.

Figure 3 illustrates the effect of the Pt-loading on the i/E relations for the h.e.r. from an electrolyte of 5 M KOH flowing at 0.88 cm s^{-1}. The figure shows only the values of E_L which are of more practical importance. The Pt-loading causes a considerable decrease in the potential required to support a certain rate of generation of hydrogen gas, particularly at higher rates (i.e., greater than 100 mA cm^{-2}). This is attributed to the better electrocatalytic activity of the platinum loading as compared to the graphite substrate. The exchange current density of the h.e.r. in 0.1 M NaOH at 25 °C is reported to be 1.16×10^{-6} and 3.9×10^{-4} A cm^{-2} on graphite and platinum, respectively [1]. It is shown below (cf. Equation 3b) that an increase in the exchange current density, i_o, and/or the specific surface area of the packed bed, S, decrease the polarization required to support a certain current output.

A significant feature was visually observed in the behaviour of the Pt-loaded graphite electrode. At low current densities, the hydrogen evolution reaction was uniformly distributed on the electrode surface, as judged from the uniform evolution of the hydrogen gas bubbles off the entire electrode surface. However,

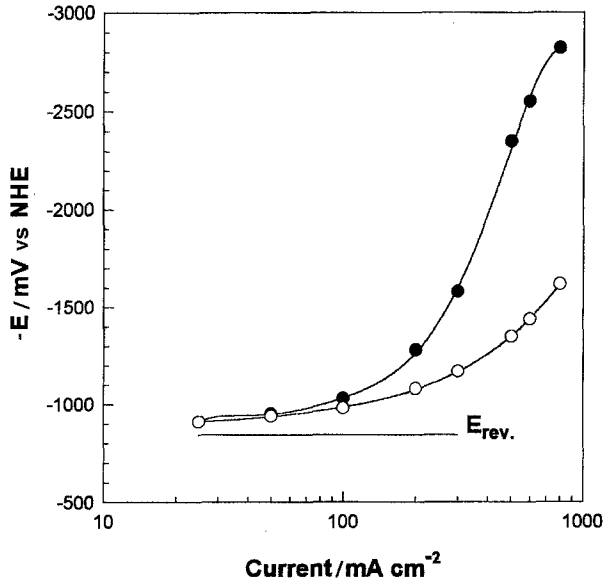

Fig. 3. Comparison of the current–potential relations for the h.e.r. on graphite and on Pt-loaded graphite electrodes in 5 M KOH at 30 °C flowing at 0.88 cm s^{-1}. Key: (●) E_L of Pt-loaded graphite; (○) E_L of unloaded graphite.

at higher current densities, the gas was seen to evolve profusely only from isolated spots on the electrode surface. These are the spots where platinum aggregates are located on the graphite surface. Figure 4 is an SEM of the Pt-loaded surface which shows the platinum aggregates on the surface. This observation indicates that the platinum loading catalyses the h.e.r. only at the external surface of the electrode.

3.2. *Mathematical modelling*

The effects of the specific surface area, exchange current density, conductivity of the gas–electrolyte dispersion filling the pore space and the structural properties of the electrode on the current–potential relations have been previously treated within the framework of a mathematical model [19]. The model was solved for the following conditions: (i) Tafelian polarization at the exit face of the electrode (η_L) and (ii) large values of ohmic potential drop within the pore electrolyte (i.e., $E_L \gg E_o$). Both conditions are not valid over the range of our experimental results. Consequently, the model must be modified to incorporate the Butler–Volmer equation instead of the Tafel equation and to retain the polarizations at both entry (η_o) and exit (η_L) faces of the electrode. The derivations are shown in Appendix 1, following the same lines as [19]. The resulting current–polarization relation is given by

$$\cosh\left(\frac{\eta_L}{2b}\right) - \cosh\left(\frac{\eta_o}{2b}\right) = \left(\frac{\Delta}{2I^2}\right)\left[\frac{2 - I\bar{i}}{(1 - I\bar{i})^{1/2}} - 2\right] \tag{3a}$$

where I, $\bar{i}$ and Δ are dimensionless quantities defined as follows. $I = i_o SL\sigma/\lambda Q$ is the product of catalytic ($i_o SL$) and transport ($\sigma/\lambda Q$) parameters, $\bar{i} = i/i_o SL$ is the dimensionless current density and $\Delta = i_o SL\rho L/b$ is the index of ohmic effect [19].

Converting Equation 3(a) into dimensional variables leads to

$$\cosh\left(\frac{\eta_L}{2b}\right) - \cosh\left(\frac{\eta_o}{2b}\right) = \frac{\rho^\circ}{bi_o S\tau^2}\left[\frac{2 - \tau i}{(1 - \tau i)^{1/2}} - 2\right] \tag{3b}$$

where i is the current density at the exit face of the electrode in A cm^{-2} of the geometrical cross-sectional area of the electrode, ρ° is the resistivity of the pore electrolyte in the absence of gas bubbles, given by $\rho^\circ = \rho_b^\circ \lambda$, where ρ_b° is the resistivity of the bulk electrolyte outside the porous medium, i_o is the exchange current density in A cm^{-2}, S is the specific surface area of the porous electrode in cm^{-1} and $\tau = \sigma/\lambda Q$ is a transport parameter in cm^2 A^{-1} [19]. This parameter converts the current density into gas void fraction through dependence on σ which is a constant ($\sigma = 0.127$ cm^3 C^{-1} for the h.e.r.), Q is the superficial velocity of the electrolyte in cm s^{-1} and $\lambda = q/\theta$ is the labyrinth factor; q and θ are the tortuousity factor and porosity of the electrode, respectively.

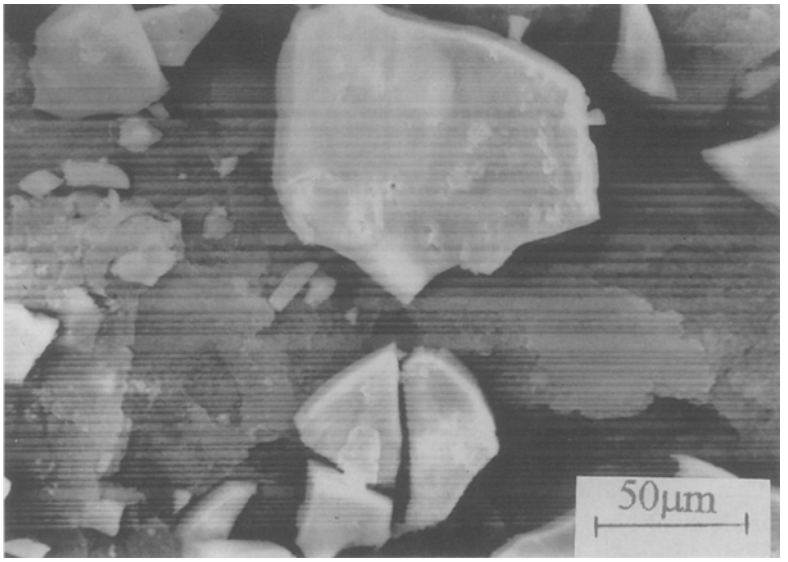

Fig. 4. SEM micrograph of the Pt-loaded graphite surface.

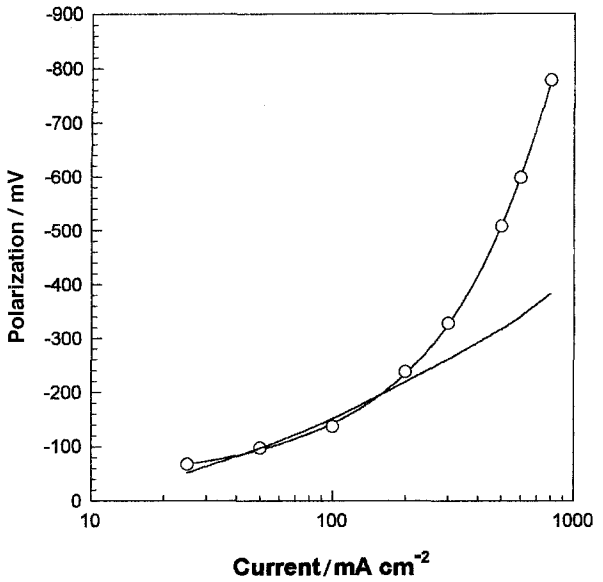

Fig. 5. Comparison between the theoretical (—) and experimental (O) current–polarization relations for the h.e.r. on Pt-loaded graphite electrode.

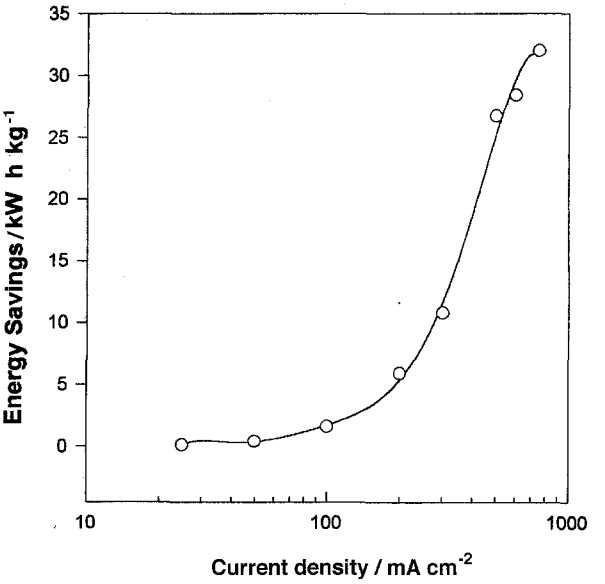

Fig. 6. Relation between the rate of power saving at the cathode upon loading with Pt against the current density.

Equation 3(b) displays the complexity of the current–polarization relation of this system. The relation is highly nonlinear and is sensitive to ρ°, i_o S and τ. At a certain set of i and τ values, an increase in (ρ°/i_oS) leads to an increase in the difference between η_L and η_o. Such an increase may result from increases in ρ° and/or decreases in i_o and/or S. Alternatively, for constant values of i, ρ°, i_o and S an increase in τ leads to a decrease in the difference between η_L and η_o. At sufficiently large values of current and polarization, the cosh function converges to an exponential function and Equation 3(b) converges to Equation 14 in [19], (see Appendix 1).

Figure 5 shows a comparison between the experimentally measured and the theoretically predicted i/E relations for the h.e.r. on Pt-loaded graphite electrode. The theoretical i/E relation was calculated using the following values: $L = 0.2\,\text{cm}$, $\rho = 1.66\,\Omega\,\text{cm}$, $\lambda Q = 0.5\,\text{cm s}^{-1}$, $i_o = 4.3 \times 10^{-6}\,\text{A cm}^{-2}$ and $S = 2.4 \times 10^3\,\text{cm}^{-1}$. The predicted i/E relation agrees with the measured relation up to current densities of about $200\,\text{mA cm}^{-2}$. Beyond this value the model predicts lower polarizations than those experimentally measured. This behaviour can be attributed to trapping of gas bubbles within the pores of the electrode. This leads to two simultaneous effects: (i) increase in the gas void fraction, ϵ, within the pores of the electrode and, hence, in its resistivity by an extent greater than that predicted by the model; and (ii) decrease of the internal surface area of the electrode in contact with the electrolyte which is accessible for the reaction leading to an increase in the corresponding activation polarization.

The value of i_oS of $1.03 \times 10^{-2}\,\text{A cm}^{-3}$ which was used in obtaining the theoretical curve of Fig. 5 is to be compared to a value of $0.936\,\text{A cm}^{-3}$ calculated using $i_o = 3.9 \times 10^{-4}\,\text{A cm}^{-2}$ as reported for the h.e.r. on the platinum electrode in 0.1 M NaOH [1], and $S = 2.4 \times 10^3\,\text{cm}^{-1}$. With the above value of i_o for the graphite used in this work, it follows that only a small fraction (about 1.1%) of the surface area of the platinum loading is being used to support the reaction.

3.3. *Energy consumption*

The significant decrease in potential brought about by the platinum loading corresponds to a reduction in the rate of energy consumption at the cathode. The energy saving in watt hours, ΔW_c, at the cathode at a particular current, i, is given by

$$\Delta W_c = \frac{i\Delta E(c)t}{3600} \tag{4}$$

where t is the electrolysis time in seconds, $\Delta E(c)$ is the decrease in potential at this particular current at the cathode brought about by the platinum loading. The values of $\Delta E(c)$ were obtained from Fig. 3. The amount of hydrogen gas produced (in g equiv.) is given by Faraday's law as (it/F). Consequently, the energy saving, P, at the cathode per gram of hydrogen gas is given by

$$P = \frac{i\Delta E(c)(t/3600)}{i(t/F)} = \frac{\Delta E(c)F}{3600} \tag{5}$$

where P is the W h per gram of hydrogen gas.

The value of P was calculated at various current densities from the data in Fig. 3 and plotted against the operating current density in Fig. 6. The energy saving per gram of hydrogen gas increases with the increase in current density. The most beneficial effect of the platinum loading appears upon operating beyond a current density of about $300\,\text{mA cm}^{-2}$, which is the range of practical importance.

References

[1] B. V. Tilak, B. P. W. T. Lu, J. E. Colman and S. Srinivasan 'Comprehensive Treatise of Electrochemistry', vol. 2 (edited by J. O'M. Bockris, B. E. Conway, E. Yeager and R. E. White), Plenum Press (1981), p. 1.

[2] D. Pletcher, 'Industrial Electrochemistry' Chapman & Hall, New York (1982), Chapter 5.

[3] A. J. Appleby and G. Crepy, *in* 'Advanced Electrolysis in Alkaline Solution'. Proceeding of the Symposium on 'Electrode Materials and Processes for Energy Conversion and Storage' (edited by J. D. E. McIntyre and S. Srinivasan), vol. 77b (1977), Chapter 4.
[4] A. J. Appleby, M. Chemla, H. Kita and G. Bronoel, *in* 'Encyclopedia of the Electrochemistry of Elements' (edited by A. J. Bard), Marcel Dekker, New York (1982), p. 556.
[5] P. Maruthamuthu and M. Ashokkumar, *Int. J. Hydrogen Energy* **14** (1989) 275.
[6] N. Tchernikovsky, P. J. Moran and E. Gileadi, *J. Electrochem. Soc.* **136** (1989) 1089.
[7] L. Chen and A. Lasia, *ibid.* **139** (1992) 3458.
[8] P. K. Wrona, A. Lasia, M. Lessard and H. Menard, *Electrochim. Acta* **37** (1992) 1283.
[9] J.-Y. Hout, *J. Electrochem. Soc.* **136** (1989) 1933.
[10] M. Szklarczyk, R. C. Kainthla and J. O'M. Bockris, *ibid.* **136** (1989) 2512.
[11] M. Okido, J. K. Depo and G. A. Capuano, *ibid.* **140** (1993) 127.
[12] L. Chen and A. Lasia, *ibid.* **138** (1991) 3321.
[13] H. Dumont, P. Los, L. Brossard, A. Lasia and H. Menard, *ibid.* **139** (1992) 2143.
[14] R. Manoharan and J. B. Goodenough, *ibid.* **139** (1990) 910.
[15] M. Matsumura, M. Hiramoto and H. Tsuubomura, *ibid.* **130** (1983) 326.
[16] J. Wang and H. D. Dewald, *ibid.* **130** (1983) 1814.
[17] I. C. Agarwal, A. M. Rochon, H. D. Gesser and A. B. Sparling, *Water Res.* **18** (1984) 227.
[18] J. Fournier, P. K. Wrona, A. Lasia, R. Lacasse, J.-M. Lalancette, H. Menard and L. Brossard, *J. Eletrochem. Soc.* **139** (1992) 2372.
[19] B. G. Ateya and B. E. El-Anadouli, *ibid.* **138** (1991) 1331.
[20] B. G. Ateya and E. S. Arafat, *ibid.* **130** (1983) 799.
[21] M. El-Shakre, M. Saleh, B. El-Anadouli and B. G. Ateya, *ibid.* **141** (1994) 441.
[22] D. Dobos, 'Electrochemical Data', Elsevier, New York (1975), pp. 55 and 85.
[23] M. M. Saleh, M. M. Khader, B. E. El-Anadouli and B. G. Ateya, *Electrochim. Acta* **36** (1991) 1899.

Appendix

This Appendix summarizes the derivation of Equation 3(a). A space element dx, as shown in Fig. 7, is considered.

We follow the same procedure as in [19], but instead of using the Tafel equation to describe the charge transfer kinetics we use the Butler–Volmer equation, that is,

$$di(x) = i_o S\left[\exp\left(\frac{\beta\eta(x)}{b}\right) - \exp\left(\frac{-\alpha\eta(x)}{b}\right)\right]dx \quad (6)$$

for the case $\alpha = \beta = 0.5$ the above relation becomes

$$di(x) = 2i_o S \sinh\left(\frac{\eta(x)}{2b}\right)dx \quad (7a)$$

The current is related to the potential gradient by Ohm's law i.e.

$$i(x) = \frac{1}{\rho(x)} \times \frac{d\eta(x)}{dx} \quad (8a)$$

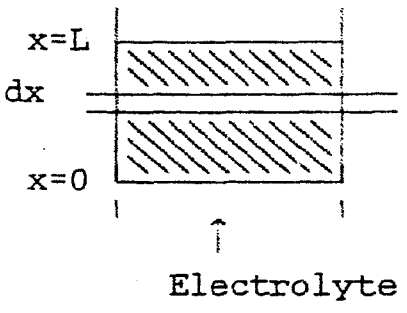

Fig. 7. Schematic of a porous electrode.

where $\rho(x)$ is the effective resistivity of the pore electrolyte at distance x within the porous electrode.

The resulting gas creates voids in the flowing electrolyte. Upon establishing the proper balance, the gas void fraction created at a distance x within the porous flow through electrode, $\epsilon(x)$ is given by [19]:

$$\epsilon(x) = \frac{\sigma}{V} \times i(x) \quad (9)$$

where σ is a characteristic constant (0.127 for the h.e.r.) and V is the superficial electrolyte flow rate.

The resistivity of the gas-electrolyte dispersion within the pore is given by Bruggemann's equation:

$$\rho = \rho^o[1 - \epsilon]^{-3/2} \quad (10a)$$

The boundary conditions are:
at $x = 0$, $i(x) = 0$; $\eta(x) = \eta(0)$
at $x = L$, $i(x) = i(L)$; $\eta(x) = \eta(L)$

Normalization of the above equations gives

$$\frac{di}{dx} = 2\sinh\left(\frac{\eta}{2}\right) \quad (7b)$$

$$i = \frac{1}{\Delta\rho} \times \frac{d\eta}{dx} \quad (8b)$$

$$\rho = (1 - \epsilon)^{-3/2} = (1 - Ii)^{-3/2} \quad (10b)$$

where $\Delta = K\rho^o L/b$, $K = i_o SL$, $I = K\tau$ and $\tau = \sigma/\lambda Q$. The objective now is to solve the above system of simultaneous nonlinear equations to obtain a relation between the current output $i(L)$ and the polarizations at both the entry (η_o) and exit (η_L) faces. Differentiating Equation 7(b) with respect to x, gives

$$\frac{d^2i}{dx^2} = \cosh\left[\frac{\eta}{2}\right] \times \frac{d\eta}{dx} \quad (11)$$

Since

$$\frac{d}{dx}\left(\frac{di}{dx}\right) = \frac{d}{dx}(Y) = \left(\frac{dY}{di}\right)\left(\frac{di}{dx}\right)$$

where $Y = di/dx = 2\sinh[\eta/2]$, then

$$dY = \cosh\left(\frac{\eta}{2}\right)d\eta$$

Thus, Equation 11 becomes

$$\cosh(\eta/2)\frac{d\eta}{dx} = \frac{dY}{di}2\sinh\left(\frac{\eta}{2}\right) \quad (12)$$

from Equations (8b) and 10(b) and by the value of dY into Equation 12

$$i\Delta(1 - Ii)^{-3/2}di = 2\sinh\left(\frac{\eta}{2}\right)d\eta \quad (13)$$

integration of the above equation leads to

$$\cosh\left(\frac{\eta}{2}\right) = \frac{\Delta}{2I^2}\frac{2 - Ii}{(1 - Ii)^{1/2}} + C \quad (14)$$

where C is the integration constant, whose value can be obtained by applying the above boundary conditions. Then Equation 14 becomes

$$\cosh\left(\frac{\eta_L}{2}\right) - \cosh\left(\frac{\eta_o}{2}\right) = \frac{\Delta}{2I^2}\left[\frac{2 - Ii(L)}{(1 - Ii(L))^{1/2}} - 2\right] \quad (15)$$